Fully Developed Temperature Waves in a Bed of Processed Shale

The combustion of processed shale is analyzed. By using a coordinate system moving with the same velocity as the combustion zone a model is obtained for the fully developed temperature wave. Of particular interest is the interpretation of this wave in terms of the kinetics and thermal effects of the reactions that are involved.

MILTIADIS HISKAKIS
and T. J. HANRATTY
Department of Chemical Engineering
University of Illinois
Urbana, IL 61801

SCOPE

In the combustion retorting of oil shale, a combustion wave is caused to move down through a bed of raw shale particles. Hot inert gases flow ahead of the wave and decompose the kerogen in the raw shale. Oil produced by this pyrolysis reaction is carried from the hot zone as a vapor, which condenses on cold shale particles and falls out the bottom of the bed as a liquid product. The pyrolysis leaves behind a bed of particles containing a carbonaceous residue (carbon with a small amount of hydrogen), a variety of carbonates, some silicates, and a large amount of inert rock. The carbonaceous residue in the processed shale provides the fuel for the combustion. The size of the oil yield from the process depends on keeping the combustion zone separated from the retorting zone and on minimizing the combustion of oil by oxygen which has bypassed the hot carbon residue.

We have been developing a simple model for this process in which the characteristics of the wave are described after it moves a sufficient distance into the bed that the reaction zones have reached fully developed conditions. The flow is assumed to be uniform and adiabatic so that the wave is one-dimensional. By using a coordinate system moving with the wave velocity the partial differential equations describing the reaction zones become ordinary differential equations. The analysis is considerably simplified by neglecting dispersion of heat and mass in the flow direction and by assuming the rock fragments are small enough that no temperature gradients exist in the solids. Since the analysis uses separate equations for the solid and the gas, effects of heat dispersion can be taken into account by adjusting the heat transfer coefficient between the solid and gas (Hiskakis and Hanratty, 1983).

In a previous paper (Hiskakis and Hanratty, 1983) results were presented for an analysis of the combustion of a bed of particles impregnated with carbon. In the present paper, this analysis is extended to particles containing carbonates and silicates; i.e., processed shale. In a third paper entitled: "Relation of Oil Yield to the Structure of the Thermal Wave in the Combustion Processing of Oil Shale," the retorting of the kerogen is included so that product yield can be related to process variables.

CONCLUSIONS AND SIGNIFICANCE

This paper presents the first calculations for the fully developed concentration and temperature profiles that are obtained from the combustion of processed shale. The structure of the temperature profile is related to the kinetics and thermal effects of the chemical reactions. An important ingredient is the suggestion that a separate thermal front moving at its own velocity can be associated with each reaction. The separation or combination of these fronts determines the temperature profile.

The parameter β, defined by Hiskakis and Hanratty (1983), is found to be useful in understanding the combustion of processed shale. The influence of the endothermic effects associated with the decomposition of calcite and dolomite are represented by dimensionless groups, N_{di}, formed with different adiabatic reaction temperatures.

Since the main exothermic and endothermic reactions involved in the retorting of oil shale are considered, the results presented could be of considerable interest in determining operating conditions which will separate the combustion and retorting regions of the temperature wave, and therefore minimize the oxygen breakthrough from the combustion region to the retorting region.

INTRODUCTION

In Hiskakis and Hanratty (1983—hereafter HH-1), as well as in a paper by Baer and Dahl (1980), the parameter $\beta = \dot{m}_g C_g / V\rho_s C_s(1-\epsilon)A$ is found to be critically important in analyzing the combustion of particles impregnated with carbon. An observer

moving with the combustion wave velocity sees the countercurrent movement of gas and solids with mass flow rates of $\dot{m}_g$ and $V\rho_s(1-\epsilon)A$. Consequently, to this observer, β may be viewed as the ratio of heat capacity of the gas flow to the heat capacity of the solid flow.

For the case of $\beta < 1$, it is shown in HH-1 that the combustion occurs in the front part of the hot zone that moves through the bed. Gas emerging from this zone heats up raw shale to the combustion temperature. Combustion proceeds until all the available carbon is consumed and the bed reaches its maximum temperature. The air entering the bed cools the inert solid that remains after the combustion is completed. The heating and combustion zone in the front of the wave has a temperature profile which does not change with time. It moves at a faster velocity than the unsteady cooling zone in the back of the wave so that a temperature plateau separates the two regions. This plateau increases in size as the wave moves through the bed so as to absorb the heat from the combustion process. Not all of the oxygen is consumed by combustion because of insufficient contact time between the oxygen and the heated particles containing carbon. This fraction of the oxygen remaining at the end of the bed is designated as η_s.

For the case of $\beta > 1$ the combustion zone occurs in the back of the hot zone. The cold gas entering the bed encounters particles impregnated with carbon, rather than inert solid, when it reaches the ignition temperature. Combustion proceeds until all the oxygen is consumed and the bed reaches its maximum temperature. The unsteady heating zone in the front of the wave moves at a faster velocity than the cooling and combustion zone so that the amount of heated inert shale increases as the wave moves through the bed. In this case a fraction of the carbon, χ_s, is bypassed by the combustion zone.

For the case $\beta = 1$, a fully developed reaction zone is never attained. The peak temperature of the wave will continue to increase as it moves through the bed.

The combustion of raw processed shale differs from the analysis presented in HH-1, in that the endothermic reactions involving the carbonate decomposition and the gasification of carbon by carbon dioxide now need to be considered.

The principle goals of this paper are to define parameters which control the combustion of a bed of processed shale particles, to provide a physical interpretation of how the structure of the heated zone is related to these parameters, and to develop some simple design criteria which will be useful to the process engineer. A secondary goal is the development of simple methods which allow the calculation of the properties of the fully developed wave that forms after a certain period of time.

DESCRIPTION OF THE WAVE FORMS

The combustion of carbon is initiated close to 580 K. It is assumed to occur according to the reaction

$$C + O_2 \rightarrow CO_2 \tag{1}$$

which is highly exothermic, releasing $|\Delta H_1| = 7{,}838$ kcal (32,816 kJ) per kg of carbon.

At high enough temperatures the carbon can react with carbon dioxide produced by the carbonate decomposition or by the carbon combustion, producing carbon monoxide:

$$C + CO_2 \rightarrow 2CO \tag{2}$$

This reaction is endothermic absorbing $|\Delta H_2| = 2{,}202$ kcal (9,219 kJ) per kg of carbon. If b = the moles of carbon consumed per mole of oxygen reacting, then $(b-1)/b$ is the fraction of carbon reacting with carbon dioxide and $1/b$ is the fraction reacting with oxygen. The combined heat effects of Reactions 1 and 2 give the heat released per kg of carbon consumed; i.e., $|\Delta H_c| = (1/b)|\Delta H_1| - (b-1)\Delta H_2$.

The raw shale contains a variety of carbonates (Campbell, 1970) that decompose at different temperatures. For simplicity only dolomite and calcite are usually considered (Mallon and Braun, 1976; Campbell and Burnham, 1979; Braun, 1981). The reaction scheme proposed by Braun (1981) is used:

$$\text{Dolomite: } MgCO_3 \rightarrow MgO + CO_2 \tag{3}$$

$$\text{Calcite: } 5CaCO_3 + 2SiO_2 \rightarrow 2Ca_2SiO_4 + CaO + 5CO_2 \tag{4}$$

Decomposition of the dolomite and the calcite absorb $\Delta H_3 = 375$ kcal/kg (1,571 kJ/kg) of $MgCO_3$ (3,000 kJ/kg of CO_2) and $\Delta H_4 = 301$ kcal/kg (1,261 kJ/kg $CaCO_3$ (2,900 kJ/kg CO_2).

For the case of $\beta < 1$ all of the carbon is consumed. From a heat balance the following final temperatures are calculated for an adiabatic system for the cases in which only the dolomite is decomposed and in which all of the calcite and dolomite are decomposed:

$$T_{ad} = T_f + \frac{|\Delta H_c|\chi_s - |\Delta H_3|\chi_d}{C_s(1-\beta)} \tag{5}$$

$$T_{adc} = T_f + \frac{|\Delta H_c|\chi_s - |\Delta H_3|\chi_d - |\Delta H_4|\chi_c}{C_s(1-\beta)} \tag{6}$$

If $\beta > 1$ a fraction of the combustible carbon, ψ_s, does not react. For this case

$$T_{ad} = T_i + \frac{|\Delta H_c|\chi_s(1-\psi_s) - |\Delta H_3|\chi_d}{C_s(\beta-1)} \tag{7}$$

$$T_{adc} = T_i + \frac{|\Delta H_c|\chi_s 1 - \psi_s - |\Delta H_3|\chi_d - |\Delta H_4|\chi_c}{C_s(\beta-1)} \tag{8}$$

Figures 1 through 6 present the different types of fully developed temperature waves that are calculated. The symbols T_s (solid line) and T_g (broken line) are respectively the temperatures of the solid and the gas. The combustion wave is moving from left to right at a velocity V. The profile is what is measured at a certain time by an observer moving with velocity V. The origin $x = 0$ is the location at which the solid starts reacting. For convenience, identify zone II where the reactions occur, zone I where only a cooling of the solids occurs, and zone III where only a heating of the solid occurs. The influence of the carbonate decomposition on these profiles can be described using the parameters

$$N_{d1} = T_{ad}/T_{df}, \tag{9}$$

$$N_{d2} = T_{adc}/T_{cf}, \tag{10}$$

for the case of $\beta < 1$, and

$$N_{d3} = T_{adc}/T_{di}, \tag{11}$$

$$N_{d4} = T_{ad}/T_{di}, \tag{12}$$

for the case of $\beta > 1$. Here T_{di} and T_{df} are the temperatures at which the dolomite present in the rock starts and stops decomposing, and T_{cf} is the temperature at which the calcite stops decomposing.

Temperatures T_{cf}, T_{df} and T_{di} are, respectively, approximately equal to 1,000, 850, and 800 K. In order to obtain more accurate values of these temperatures it is necessary to use the kinetic equations for the decompositions. From the equilibrium for calcite decomposition,

$$T_{cf} = \frac{E_4}{-R \ln\left[\dfrac{\dfrac{d\gamma}{dx}V}{\gamma A_4}\right]}, \tag{13}$$

$$\frac{d\gamma}{dx} \rightarrow 0 \qquad \gamma = \gamma_s,$$

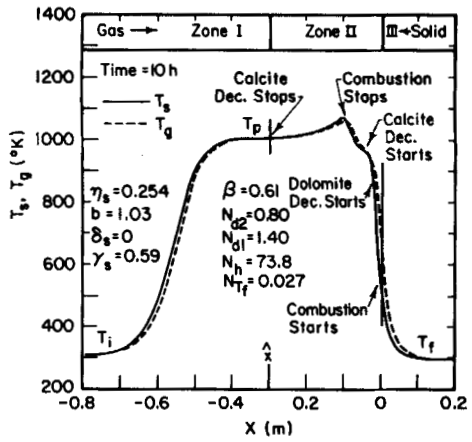

Figure 1a. Temperature profile for a plug flow processed shale with $\beta < 1$, $N_{d2} < 1$, $N_{d1} > 1$.

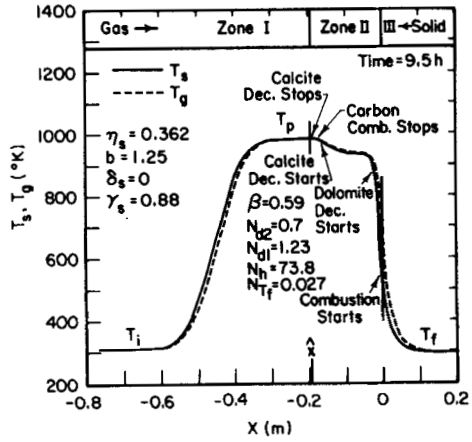

Figure 1b. Temperature profile for processed shale combustion with $\beta < 1$, $N_{d1} > 1$, $N_{d2} < 1$ (O_2 diffusion inhibited by CO_2 generation).

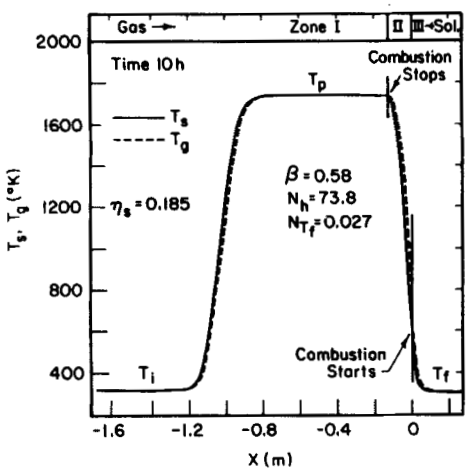

Figure 1c. Temperature profile for the combustion of a processed free of carbonate shale.

where γ is the fraction of calcite remaining and γ_s is defined from heat balance Eq. 26. The dolomite decomposition equation gives

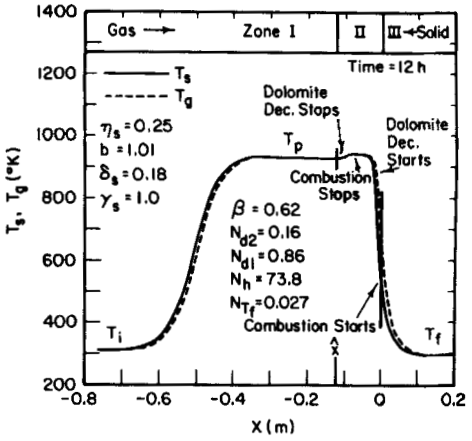

Figure 2. Temperature profile for a plug flow processed shale combustion with $\beta < 1$, $N_{d1} > 1$.

$$T_{di} = \frac{E_3}{-R \ln\left[\dfrac{\dfrac{d\delta}{dx} V}{\delta A_3}\right]}, \qquad (14)$$

$$\frac{d\delta}{dx} \to 0 \qquad \delta = 1,$$

$$T_{df} = \frac{E_3}{-R \ln\left[\dfrac{\dfrac{d\delta}{dx} V}{\delta A_3}\right]}, \qquad (15)$$

$$\frac{d\delta}{dx} \to 0 \qquad \delta = \delta_s,$$

where δ is the fraction of calcite remaining and δ_s is defined by heat balance Eq. 25.

Consider first cases of $\beta < 1$ (Figures 1a, 2, 3) for which the combustion occurs in the front part of the wave. Zone I may be visualized as an unsteady cooling wave, which, with increasing time, becomes more diffuse, and zone III is a steady state heating wave. For $\beta < 1$ not all the oxygen need be consumed. A fraction, η_s, of the initial oxygen bypasses the combustion zone.

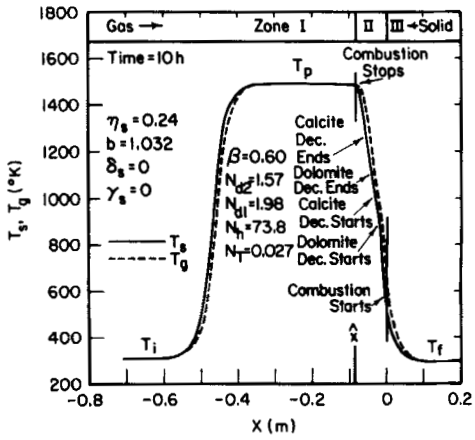

Figure 3. Temperature profile for a plug flow processed shale combustion with $\beta < 1$, $N_{d2} > 1$.

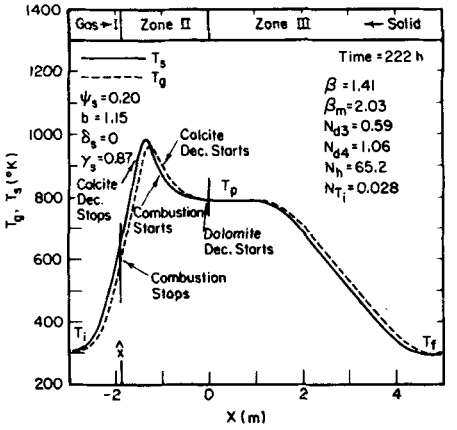

Figure 4. Temperature profile for a plug flow processed shale combustion with $\beta > 1$, $N_{d4} > 1$, $N_{d3} < 1$.

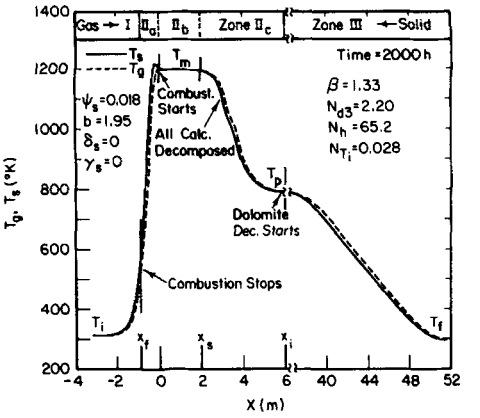

Figure 6. Temperature profile for a plug flow processed shale combustion with $\beta > 1$, $N_{d3} > 1$.

For $N_{d2} < 1$ (Figures 1a and 2) the heat released by combustion is not enough to decompose all the carbonates. It is noted that after the combustion terminates, carbonates continue to decompose. Consequently, the maximum temperature reached by the bed is larger than the plateau temperature, T_p. For Figure 1a, $N_{d1} > 1$, all of the dolomite decomposes and a fraction, γ_s, of the calcite does not react. The decomposition terminates when the temperature reached $T_p = T_{cf}$. For $N_{d1} < 1$ (Figure 2), none of the calcite and only a fraction of the dolomite, $(1 - \delta_s)$, decomposes. Consequently the decomposition of the carbonates terminate at $T_p = T_{df}$.

For $N_{d2} > 1$ (Figure 3) all of the carbonates decompose. Consequently the maximum temperature is reached when all of the carbon is consumed and $T_p = T_{adc}$.

If $\beta > 1$ the combustion occurs in the back of the thermal zone. All of the oxygen and only a fraction of the carbon, $(1 - \psi_s)$, is consumed. Figures 4, 5 and 6 show typical $\beta > 1$ waves. Zone III is now an unsteady heating wave and zone I is a steady state cooling wave. The hot inert gases moving ahead of the combustion zone to provide heat for the decomposition of the carbonates as well as for the gasification of carbon by carbon dioxide. The fraction of the carbon reacting with CO_2, $(b - 1)/b$, can be larger in these cases because of the long contact time of the CO_2 from carbonate decomposition with hot carbon.

For $N_{d4} > 1$ and $N_{d3} < 1$ (Figure 4), all of the dolomite and a fraction, $1 - \gamma_s$, of the calcite is decomposed. In the downstream part of the reaction zone only dolomite decomposition occurs because there is no oxygen left in the gas flow to cause carbon combustion. The plateau temperature equals the temperature required to initiate dolomite decomposition, $T_p = T_{di}$.

For $N_{d3} < 1$ and $N_{d4} < 1$ (Figure 5) none of the calcite and a fraction of the dolomite, $1 - \delta_s$, is decomposed. Again $T_p = T_{di}$. However, in this case the peak gas temperature is smaller than for $N_{d4} > 1$, $N_{d3} < 1$.

For $N_{d3} > 1$ (Figure 6) all of the dolomite, $\delta_s = 0$, and calcite, $\gamma_s = 0$, decomposes. A very different situation develops than for $N_{d3} < 1$. An additional plateau at T_m appears that separates the carbonate decomposition from the combustion zone. Because the bed reaches such a high temperature and because the time of contact of CO_2 with the carbon is very long, a considerable fraction of the carbon, $(b - 1)/b$, reacts with CO_2.

A resume of all the cases considered above is presented in Figure 7.

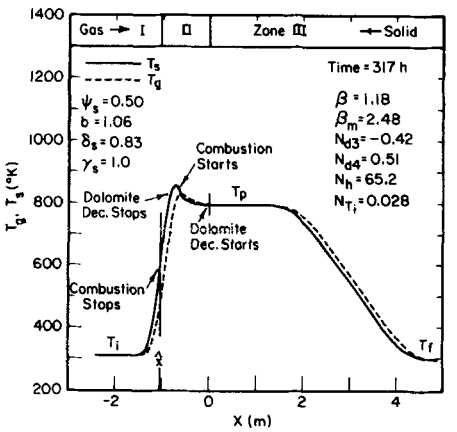

Figure 5. Temperature profile for a plug flow processed shale combustion with $\beta > 1$, $N_{d4} < 1$.

INTERPRETATION

Wave Velocities

A convenient way of interpreting the wave forms shown in Figures 1–6 is to consider the velocities of the thermal and reaction waves that can exist for such a system.

The combustion wave moves by burning carbon. Therefore, an overall mass balance for the carbon consumption will give its velocity

$$V = \frac{3bN_o\dot{m}_g(1 - \eta_s)}{8\rho_s\chi_s A(1 - \epsilon)(1 - \psi_s)}, \tag{16}$$

where N_o is the weight fraction of oxygen in the entering gas, χ_s is the weight fraction of carbon in the processed shale, and $(1 - \psi_s)$ is the fraction of the carbon consumed.

As shown in HH-1, the unsteady state heating or cooling wave moves with a velocity, V_{us}, which is calculated from an overall heat balance:

$$V_{us} = \frac{\dot{m}_g C_g}{\rho_s C_s A(1 - \epsilon)}. \tag{17}$$

From the definition of β,

$$V_{us} = \beta V. \tag{18}$$

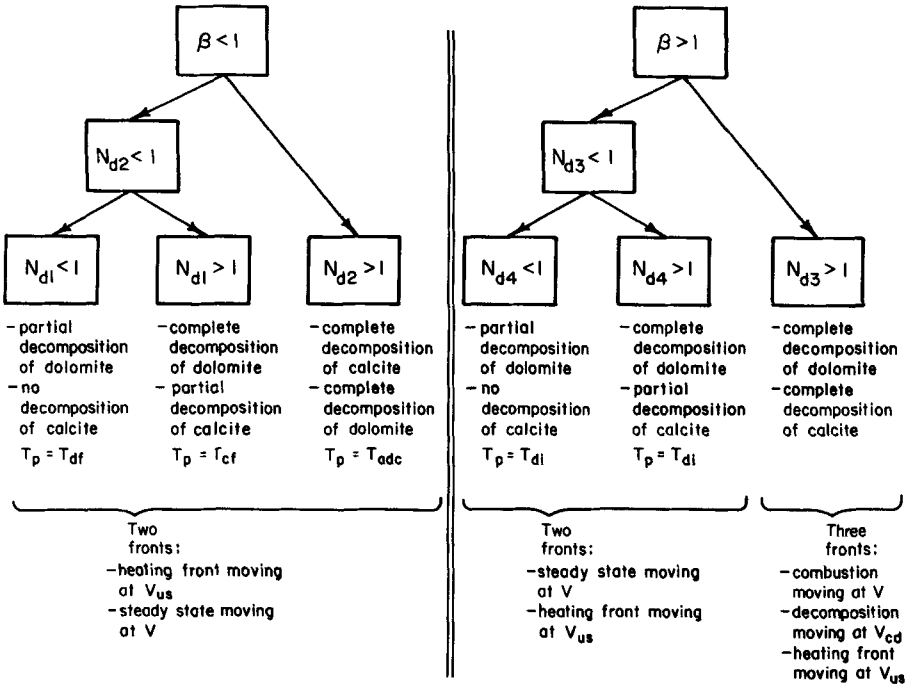

Figure 7. Cases considered in analyzing wave forms.

For $\beta < 1$, the unsteady cooling wave moves slower than the combustion wave and for $\beta > 1$, the unsteady cooling wave moves faster than the combustion wave. The distance between the two waves increases at a rate of $|1 - \beta|V$.

The inclusion of carbonate decomposition introduces other possible waves. Consider a bed containing dolomite and carbon which is initially at a temperature T_{di}. The use of a hot gas at a temperature $T_m > T_{di}$ to decompose the dolomite will produce a thermal wave moving at a velocity V_d, given by the following expression:

$$V_d = \frac{\dot{m}_g C_g}{A\rho_s C_s(1-\epsilon)} \frac{1}{1 + \dfrac{|\Delta H_3|\chi_d + |\Delta H_2|\chi_s(1-\psi_s)}{C_s(T_m - T_{di})}}, \quad (19)$$

where ψ_s is the fraction of carbon remaining after the gasification of the carbon by the CO_2 produced by the dolomite decomposition. Similarly, the thermal decomposition of a bed containing only calcite and carbon at a temperature T_{ci} with a gas at T_m will produce a decomposition wave moving at a velocity, V_c, where

$$V_c = \frac{\dot{m}_g C_g}{A\rho_s C_s(1-\epsilon)} \frac{1}{1 + \dfrac{|\Delta H_4|\chi_c + |\Delta H_2|\chi_s(1-\psi_s)}{C_s(T_m - T_{ci})}} \quad (20)$$

For the thermal decomposition of a bed of processed shale (containing dolomite, calcite, and carbon) that is initially at a temperature T_{di} and is retorted by a gas at T_m, a wave moving at V_{cd} can be defined, where

$$V_{cd} = \frac{\dot{m}_g C_g}{A\rho_s C_s(1-\epsilon)} \times \frac{1}{1 + \dfrac{|\Delta H_3|\chi_d + |\Delta H_4|\chi_c + |\Delta H_2|\chi_s(1-\psi_s)}{C_s(T_m - T_{di})}}. \quad (21)$$

Because the calcite decomposition occurs at a higher temperature than the dolomite decomposition, the calcite decomposition front can never move faster than the dolomite decomposition front. Therefore for the case where $V_c > V_d$ the calcite and dolomite decomposition waves are combined into one wave moving at a velocity V_{cd} given by Eq. 21.

The combustion wave cannot move faster than the decomposition waves because the temperature rise due to the combustion will cause the carbonates to decompose. Therefore a zone of carbonate decomposition and combustion will move at a velocity V, Eq. 16. This is the case of $\beta < 1$ (Figures 1–3).

For the case of $N_{d3} < 1$, $\beta > 1$ in Figures 4 and 5, $V_{us} > V$ and $V > V_d > V_{cd}$. Consequently, the only wave that can separate from the combustion wave is the unsteady heating wave. For the case of $\beta > 1$, $N_{d3} > 1$ in Figure 6, $V_{us} > V_{cd} > V$. Consequently, both an unsteady heating wave and a reaction wave involving dolomite and calcite decomposition can separate from the combustion wave.

Overall Heat Balances

In the case of $\beta < 1$ all the reactions take place in the same front (zone II). The combustion reaction is raising the temperature of the solid above the temperature T_{di} where the dolomite starts to decompose. The decomposition of the dolomite absorbs part of the heat released by the combustion. If, after all the carbon is consumed, the heat is not sufficient to decompose all the dolomite ($N_{d1} < 1$; Figure 2), the temperature of the solid will drop to a level (T_{df}) at which the dolomite decomposition reaction will stop. From an overall heat balance the following expression is obtained:

$$T_{df} = T_f + \frac{|\Delta H_c|\chi_s - |\Delta H_3|\chi_d(1-\delta_s)}{C_s(1-\beta)}. \quad (22)$$

By solving Eqs. 22 and 15 for δ_s, the fraction of dolomite decomposing ($1 - \delta_s$) can be calculated.

Because the calcite decomposition reaction has a higher activation energy than the dolomite decomposition, all the dolomite is decomposed before the calcite decomposition starts. In the case where the combustion reaction releases enough heat to decompose

all the dolomite ($N_{d1} > 1$) but not all the calcite ($N_{d2} < 1$; Figure 1), the solid temperature will drop to T_{cf} quenching the calcite decomposition reaction. From an overall heat balance the following expression is obtained:

$$T_{cf} = T_f + \frac{|\Delta H_c|\chi_s - |\Delta H_3|\chi_d - |\Delta H_4|\chi_c(1-\gamma_s)}{C_s(1-\beta)}, \quad (23)$$

By solving Eqs. 23 and 13 the fraction of the calcite remaining, γ_s, is calculated.

If the carbon combustion reaction can release enough heat to decompose all the carbonates $N_{d2} > 1$ (Figure 3), an overall heat balance can be used to calculate the maximum temperature of the bed.

$$T_m = T_f + \frac{|\Delta H_c|\chi_s - |\Delta H_3|\chi_d - |\Delta H_4|\chi_c}{C_s(1-\beta)}, \quad (24)$$

In the case of $\beta > 1$, the hot gas emerging from the combustion zone heats up the solid to a temperature T_{di} where the dolomite decomposition reaction starts. If the combustion cannot provide enough heat to decompose all the dolomite, $N_{d4} < 1$, the following overall heat balance and Eq. 15 can be used to calculate the dolomite remaining, δ_s:

$$T_{di} = T_i + \frac{|\Delta H_c|\chi_s - |\Delta H_3|\chi_d(1-\delta_s)}{C_s(\beta-1)}. \quad (25)$$

If the heat released by the combustion is sufficient to decompose all the dolomite, $N_{d4} > 1$, but not all the calcite, $N_{d3} < 1$, the calcite remaining, γ_s, can be calculated from the following overall heat balance equation and Eq. 13:

$$T_{di} = T_i + \frac{|\Delta H_c|\chi_s - |\Delta H_3|\chi_d - |\Delta H_4|\chi_c(1-\gamma_s)}{C_s(\beta-1)}. \quad (26)$$

In the case where the combustion reaction can release enough heat to decompose all the carbonates, $N_{d3} > 1$ (Figure 6), the combustion front (zone IIa) is separated from the decomposition front (zone IIc) by a long plateau. The temperature of this plateau, T_m, can be obtained from an overall heat balance for the combustion zone:

$$T_m = T_i + \frac{|\Delta H_c|\chi_s(1-\psi_s)}{C_s(\beta-1)} \quad (27)$$

NUMERICAL RESULTS

Heat Balance Equations

The heat balance equations used to calculate the gas phase and solid phase temperature profiles shown in Figures 1–6 are as follows:

$$\rho_g \epsilon C_g \frac{\partial T_g}{\partial t} = h_{gs}a_p(1-\epsilon)(T_s - T_g) - \frac{\dot{m}_g}{A} C_g \frac{\partial T_g}{\partial z}, \quad (28)$$

$$\rho_s(1-\epsilon)C_g \frac{\partial T_s}{\partial t} = -h_{gs}a_p(1-\epsilon)(T_s - T_g) - (1-\epsilon)\rho_s \Sigma_i \Delta H_i r_i \chi_i \quad (29)$$

Here, h_{gs} is the heat transfer coefficient between the gas and the solid, r_i is the rate of disappearance of a species by chemical reaction, ΔH_i is the heat effects associated with that reaction, and χ_i is the weight fraction of the species in the solid. For simplification, fluid properties have been assumed constant and dispersion has been neglected. The justification for making these assumptions is presented in HH-1.

If it is assumed that the temperature field is steady to an observer moving with velocity V, the partial differential Eqs. 28 and 29 are changed to ordinary differential equations:

Table 1. Influence of Dimensionless Groups on Degree of Completion of Reactions

	β	N_h	N_{Tf}	N_{Ti}	N_{d1}	N_{d2}	N_{d3}	N_{d4}
η_s	X	X	X	—	—	X	—	—
ψ_s	X	X	—	X	—	—	X	—
b	X	—	—	—	—	X	X	—
δ_s	X	—	—	—	X	X	X	X
γ_s	X	—	—	—	X	X	X	X

$$-\frac{\dot{m}_g}{A} C_g \frac{dT_g}{dx} + h_{gs}a_p(1-\epsilon)(T_s - T_g) = 0, \quad (30)$$

$$V\rho_s C_s(1-\epsilon)\frac{dT_s}{dx} - h_{gs}a_p(1-\epsilon)(T_s - T_g) - (1-\epsilon)\rho_s \Sigma_i \Delta H_i r_i \chi_i = 0. \quad (31)$$

Equations 28 and 29 are used to calculate the temperature profiles in unsteady state cooling and heating zones (zone I for $\beta < 1$, zone III for $\beta > 1$) by using $r_i = 0$. Equations 30 and 31 are used for all other zones. Methods for solving these equations and for matching solutions for the different zones are given in Appendix 1.

Parametrization of the Problem

The parameters which characterize the degree of completion of the reactions are η_s, ψ_s, b, δ_s, and γ_s. As summarized in Table 1, these are functions of the dimensionless groups β, N_h, N_{Tf}, and N_{Ti} defined in HH-1 and the new dimensionless groups defined in this paper to characterize the influence of carbonate decomposition, N_{d1}, N_{d2}, N_{d3}, and N_{d4}.

The heat exchange group N_h is given by

$$N_h = \frac{h_{gs}a_p R_p^2}{\overline{D}_e C_g \rho_g}, \quad (32)$$

where $\overline{D}_e$ is the average value of the oxygen diffusion coefficient, D_e. The groups N_{Tf} and T_{Ti} characterize the quench of the combustion reaction for the case of $\beta < 1$ and $\beta > 1$, respectively, and are defined as

$$N_{Tf} = \frac{T_f R}{E_1}, \quad (33)$$

Table 2. Values Used for Our Calculations

ρ_g	= 0.44 kg/m^3 (Perry, 1969)
C_g	= 0.523 kcal/kgK (2.2 kF/kJK) (Perry, 1969)
C_s	= 0.305 kcal/kgK (1.27 kJ/kgK)
K_g	= 60 m/h (De-Acetis and Thodos, 1960)
χ_s	= 2.21 10^{-4} (Fisher assay in 1/t) + 2.389 10^{-3} (Probstein and Hick, 1982)
χ_d	= 1.38 10^{-2} (wt % acid-evolved CO_2) (Mallon and Braun, 1976)
χ_c	= 7.76 10^{-3} (wt % acid-evolved CO_2) (Mallon and Braun, 1976)
A_1	= 9.01 10^8 h^{-1} = 2.5 10^5 s^{-1} (Sohn and Kim, 1980)
E_1	= 22,020 kcal/kmol = 92,190 kJ/kmol (Sohn and Kim, 1980)
ΔH_1	= kcal/kg C = 32,816 kJ/kg C (Gregg and Edgar, 1978)
A_2	= 2.05 10^8 h^{-1} = 5.7 10^4 s^{-1} (Braun, 1981)
E_2	= 40,260 kcal/kmol = 168,600 kJ/kmol (Braun, 1981)
ΔH_2	= 2,202 kcal/kg C = 9,219 kJ/kg C
A_3	= 6.12 10^{13} h^{-1} = 1.7 10^{10} s^{-1} (Campbell, 1978)
E_3	= 57,800 kcal/kmol = 242,000 kJ/kmol (Campbell, 1978)
ΔH_3	= 375 kcal/kg $MgCO_3$ = 3.10^6 J/kg CO_2 (Campbell, 1978)
A_4	= 3.456 10^{14} h^{-1} = 9.6 10^{10} s^{-1} (Braun, 1981)
E_4	= 72,100 kcal/kmol = 301,860 kJ/kmol (Braun, 1981)
ΔH_4	= 301 kcal/kg $CaCO_3$ = 2.9 10^6 J/kg CO_2 (Braun, 1981)

TABLE 3. NUMERICAL RESULTS OF OUR MODEL FOR $\beta < 1$

Temp. Profile	Fig. 1a	Fig. 1b	Fig. 1c	Fig. 2	Fig. 3
χ_s	0.0244	0.0244	0.0244	0.0244	0.0244
N_o	0.23	0.23	0.23	0.23	0.23
$\dot{m}_g/A$ (kg/hm^2)	47	47	47	47	47
Carbonate content (% wt fct)	36	36	0.00	58	11
β	0.61	0.59	0.58	0.62	0.60
N_{d2}	0.80	0.70	—	0.16	1.57
N_{d1}	1.40	1.23	—	0.86	1.98
N_h	73.8	73.8	73.8	73.8	73.8
N_{Tf}	0.027	0.027	0.027	0.027	0.027
β_m	0.47	0.47	0.47	0.47	0.47
N_{d2m}	0.72	0.72	—	0.22	1.30
η_s	0.254	0.362	0.185	0.25	0.24
b	1.03	1.25	1.00	1.01	1.032
δ_s	0.00	0.00	—	0.18	0.00
γ_s	0.59	0.88	—	1.00	0.00
T_p (K)	1,000	985.	1,740	912	1,495
V (m/h)	0.112	0.116	0.119	0.111	0.115

$$N_{Ti} = \frac{T_i R}{E_1} . \tag{34}$$

Temperature Profiles

The temperature profiles shown in Figures 1–6 were calculated with the equations developed in Appendix 1 using the physical properties in Table 2. A summary of the parameters characterizing these profiles, as well as some of the results, is given in Tables 3 and 4.

Figure 1a corresponds to the combustion of a Green River processed shale that has the same characteristics as the shale used in experiment S-11 performed in Lawrence Livermore Laboratory (Campbell, 1981). Figures 2, 1a, 3, and 1c show the effect of decreasing the carbonate content of the shale (58% in Figure 2, 36% in Figure 1a, 11% in Figure 3, 0% in Figure 1c). All other characteristics are the same as in the case of Figure 1a. The change in the carbonate content is reflected in the values of N_{d1} and N_{d2}. The presence of carbonates greatly alters the temperature profiles, as can be seen by comparing Figure 1c (no carbonates) to Figure 1a (36% carbonates). All cases show a thermal wave with a plateau region which broadens as the wave moves into the bed. However, the presence of carbonates greatly lowers the plateau temperature and causes a secondary peak in the front of the wave. This peak occurs approximately at the place where the combustion of carbon stops. The decrease of the bed temperature from this peak temperature to the plateau temperature, T_p, is caused by the endothermic effects associated with the carbonate decomposition.

The carbonate decomposition creates an outward flow of CO_2. This flow can hinder the oxygen diffusion into the particle. To account for this Sohn and Braun (1982) proposed a correction for the diffusion coefficient of the oxygen. To study the effect of this correction the temperature profiles in Figure 1b were calculated. This figure is to be compared directly to Figure 1a that treats the same case but without using the correction. This is the only case for which this correction is used. The justification for not including it in all calculations will be presented in the discussion section.

Figures 4 and 5 correspond to the temperature profiles developed during the combustion of a Green River processed shale with $\beta > 1$. The shale used for these cases is similar to that used for the experiment S-19 performed in Lawrence Livermore Laboratory (Campbell, 1981). The difference between the two cases in Figures 4 and 5 is that the oxygen concentration was modified in the incoming gas (2.5% O_2 by volume in the gas for Figure 4; 2% O_2 by volume in the gas for Figure 5). This change is reflected in the values of β, N_{d3}, and N_{d4}. The decrease of the oxygen (increase of β) increases the carbon breakthrough. Therefore less heat is released and the peak temperature of the bed decreases. For the same reason less carbonates are decomposed. Although the peak temperatures for Figure 4 and 5 are different, the plateau temperatures T_p are the same and are equal to T_{di}. The hot inert gas coming from the combustion zone is cooled down by the cold incoming solid to a temperature T_{di} at which the dolomite decomposition reaction stops.

Figure 6 considers a shale much richer than the shales used in the calculations presented in the previous figures (Fisher assay = 140 l/t compared to 99 l/t for the other cases). The shale contains only 11% by weight carbonates (compared to 36% for Figures 4 and 5). The oxygen content in the retorting gas is 2.5% by volume. These characteristics correspond to a shale rich in carbon and low in carbonates. Because more energy is released (more carbon and less carbonates than in all the other cases) the carbonates completely decompose. This decomposition zone (IIc) moves ahead of com-

TABLE 4. NUMERICAL RESULTS OF OUR MODEL FOR $\beta > 1$

Temp. Profile	Fig. 4	Fig. 5	Fig. 6
χ_s	0.024	0.024	0.033
N_o	0.028	0.023	0.028
$\dot{m}_g/A$ (kg/hm^2)	112	112	112
Carbonate content (% wt fct)	36	36	11
β	1.41	1.18	1.33
N_{d3}	0.59	−0.42	2.20
N_{d4}	1.06	0.51	—
N_h	65.2	65.2	65.2
N_{Tf}	0.028	0.028	0.028
β_m	2.03	2.48	2.76
N_{d3m}	0.65	0.56	—
N_{d3m}	—	—	2.02
ψ_s	0.20	0.50	0.18
b	1.15	1.06	1.95
δ_s	0.00	0.83	0.00
γ_s	0.87	1.00	0.00
T_p (K)	791	794	791
T_m (K)	—	—	1,197
V (m/h)	0.062	0.074	0.065
V_{cd} (m/h)	—	—	0.067

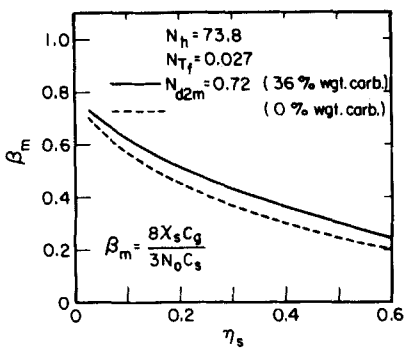

Figure 8. Effect of β_m on the oxygen breakthrough for $\beta < 1$.

bustion zone (IIa). Zone III is separated from zone II by a plateau whose length increases at a rate of $V_{us} - V_{cd}$. The temperature of the plateau, T_p, is equal to T_{di}, at which the dolomite decomposition starts.

Oxygen and Carbon Breakthrough

For $\beta < 1$ the oxygen breakthrough (η_s) decreases if $\beta \rightarrow 1$, N_h decreases or N_{Tf} increases (HH-1). If N_{d2} increases (less carbonate in the shale), the peak temperature of the bed increases and the length of the bed for which the combustion takes place increases. Therefore more oxygen is consumed during the combustion and the oxygen breakthrough decreases.

The fraction of carbon that reacts with CO_2, and is not available to the oxygen, increases (b increases) if the length of the reaction zone and the temperature of the bed is increased. Decreasing the carbonate concentration (high N_{d2}) causes a decrease in the CO_2 released, but it also causes an increase in the bed temperature. Because there is an excess of CO_2, the limiting factor in the carbon-carbon dioxide reaction is usually the temperature. As the carbonate concentration in the shale decreases (large values of N_{d2}) the CO_2 concentration becomes the limiting factor in the C-CO_2 reaction and b slowly decreases.

For $\beta > 1$, the carbon breakthrough ψ_s decreases when $\beta \rightarrow 1$, N_h decreases or N_{Ti} increases (HH-1). If N_{d3} increases (less carbonates in the shale) the peak temperature of the bed increases. This causes a larger fraction of carbon to react with CO_2 (increase in b) and consequently decreases considerably the carbon breakthrough (ψ_s). The amount of carbon reacting with carbon dioxide, and consequently b, increases if $\beta \rightarrow 1$ or N_{d3} increases.

Calcite and Dolomite Decomposition

The difference between the heat released from the exothermic combustion and the endothermic decompositions and gasification reactions dictates the amount of dolomite and calcite that decomposes. From the kinetics of the dolomite and calcite decomposition it is seen that all the dolomite decomposes before the calcite starts to decompose.

For $\beta < 1$, $N_{d1} < 1$ the heat released by the exothermic combustion is not sufficient to decompose all the dolomite. If $N_{d1} > 1$ but $N_{d2} < 1$ all the dolomite will be decomposed but only part of the calcite ($\delta_s = 0$). If $N_{d2} > 1$ all the carbonates will decomposed ($\delta_s = 0$, $\gamma_s = 0$).

For $\beta > 1$, $N_{d4} < 1$ part of the dolomite is decomposed and none of the calcite. If $N_{d4} > 1$ and $N_{d3} < 1$, all the dolomite ($\delta_s = 0$) but only part of the calcite is decomposed. For $N_{d3} > 1$ all the carbonates are decomposed ($\delta_s = 0$, $\gamma_s = 0$).

These results are also summarized in Figure 7.

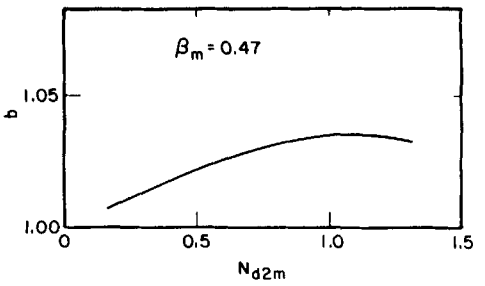

Figure 9. Effect of N_{d2m} on b for $\beta < 1$.

DESIGN CONSIDERATIONS

The main characteristics of the fully developed temperature and composition profiles can be estimated from very simple relations based on heat and mass balances. In order to use these relations one needs to know η_s (or ψ_s) and b. As we can see from Table 1, these parameters depend on the dimensionless groups β, N_h, N_{Tf}, N_{Ti}, N_{d2}, and N_{d3}. Groups β, N_{d2}, and N_{d3} cannot be calculated a priori, because they are functions of the plural η_s, ψ_s, and b. Therefore it is convenient to define a set of modified dimensionless groups β_m, N_{d2m}, N_{d3m}, and N'_{d3m}.

Parameter β_m is obtained by setting $\eta_s = 0$, $\psi_s = 0$, and $b = 1$ in the expression for β.

$$\beta_m = \frac{8\chi_s C_g}{3N_o C_s} = \frac{\beta(1-\eta_s)}{b(1-\psi_s)} \tag{35}$$

Parameters N_{d2m} and N_{d3m} are obtained from N_{d2} and N_{d3} setting $\beta = \beta_m(\eta_s = 0, \psi_s = 0, b = 1)$, and $T_{cf} = 1{,}000$ K, $T_{di} = 800$ K.

$$N_{d2m} = \frac{T_f}{1{,}000} + \frac{|\Delta H_1|\chi_s - |\Delta H_3|\chi_d - |\Delta H_4|\chi_c}{1{,}000\, C_s(1-\beta_m)} \tag{36}$$

$$N_{d3m} = \frac{T_i}{800} + \frac{|\Delta H_1|\chi_s - |\Delta H_3|\chi_d - |\Delta H_4|\chi_c}{800\, C_s(\beta_m - 1)} \tag{37}$$

In the case of $\beta > 1$, $N_{d3} > 1$ the value of b is closer to 2 than to 1. Therefore a new dimensionless group N'_{d3m} has to be defined as follows:

$$N'_{d3m} = \frac{T_i}{800} + \frac{|\Delta H_1 + \Delta H_2|\chi_s - |\Delta H_3|\chi_d - |\Delta H_4|\chi_c}{800\, C_s(2\beta_m - 1)} \tag{38}$$

This new set of modified dimensionless groups can be used to correlate the results of the numerical calculations in plots similar to Figures 8, 9, and 10. By using correlations of this type one can obtain the values for η_s, ψ_s, and b for a set of operating conditions. These can then be used to calculate characteristics of the temperature and composition profiles from overall heat and mass balances presented in the interpretation section.

The use of these relations is best illustrated by the following example: Consider the case of Figure 1a for a processed shale of Fisher assay = 99.7 l/t, $\chi_s = 0.0244$. The acid-evolved CO_2 from the shale is 16.78% by weight ($\chi_d = 0.232$, $\chi_c = 0.13$) and the retorting gas contains 23.3% oxygen by weight. Therefore, from Eq. 35, $\beta_m = 0.47$; from Eq. 32, $N_h = 73.8$ (we used $\overline{D}_e = 0.03$ m^3/h, $h_{gs} = 17$ kcal/h m^2 K, $R_p = 0.01$ m); from Eq. 33, $N_{Tf} = 0.027$ ($T_f = 295$ K); and from Eq. 36, $N_{d2m} = 0.72$. Using Figure 7 we determine $\eta_s = 0.25$ and from Figure 8, $b = 1.03$. Using Eq. 16, V = 0.11 m/h ($\rho_s = 2{,}223$ kg/m^3, $\dot{m}_g/A = 47$ kg/h·m^2) and $\beta = 0.61$. From Eq. 15, $T_{df} = 850$ K and from Eq. 13, $T_{cf} = 1{,}010$ K. From Eqs. 10 and 11, $N_{d1} = 1.40$ and $N_{d2} = 0.80$. Therefore $\delta_s = 0$ and from Eq. 23, $\gamma_s = 0.55$, $T_p = T_{cf} = 1{,}010$ K. The differences between the values calculated and the values presented in Table 3

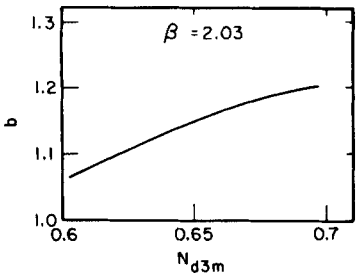

Figure 10. Effect of N_{d3m} on b for $\beta > 1$.

TABLE 5. COMPARISON OF OUR MODEL CALCULATIONS WITH OTHERS' EXPERIMENTAL AND PREDICTED RESULTS

	Combustion of Pyrolysed Shale (Fig. 1a)	Retorting S-11* Experimental Results	Retorting S-11* Braun's Model** (Fig. 11)
η_s	0.254	—	0.25†
V (m/h)	0.112	0.110	0.119
T_p (K)	1,000	1,229	1,123
b	1.03	1.08	1.07
δ_s	0.00	~0.00	0.00
γ_s	0.59	~0.00	0.00

* Livermore Lab. experimental run S-11; Campbell (1981).
** Braun (1981).
† This value refers to fraction of initial oxygen consumed by combustion of oil produced, not to actual oxygen that bypasses the bed.

(Figure 1a) are not important. These differences are due to the method used to estimate T_{cf} from Eq. 13.

DISCUSSION

Comparison with Experimental Results and Braun's Model

To our knowledge, experimental results on the burning of a bed of pyrolyzed shale are not available. Therefore, results presented in this paper are compared with those obtained for the retorting

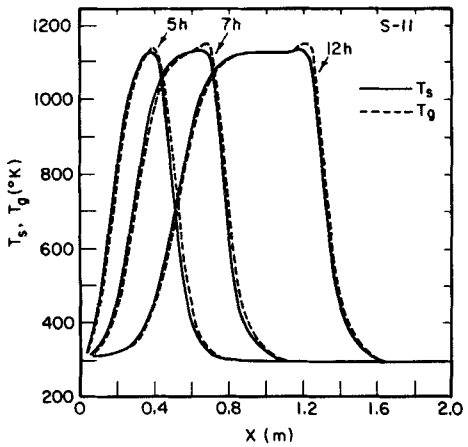

Figure 11. Temperature profile for retort S-11 (Campbell, 1981) according to Braun's (1981) model.

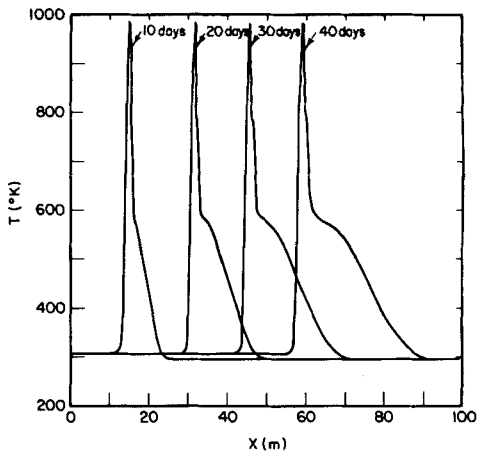

Figure 12. Temperature profile for retorting of oil shale with $\beta > 1$, $N_{d3} < 1$, $N_{d4} > 1$, according to Braun's (1981) model.

of raw shale, since the basic exothermic reactions are the same. In cases where the experimental results are incomplete or nonexistent these retorting experiments are simulated by using Braun's (1981) model.

Calculations for $\beta < 1$ were for a pyrolyzed shale of the type used in experiment S-11 performed at the Lawrence Livermore Laboratory (Campbell, 1981). In Table 5 our results (Figure 1a) are compared with those obtained in run S-11 and with the results predicted from Braun's model for the same experiment (Figure 11). The most important differences are in the plateau temperature, T_p, and the undecomposed calcite, γ_s. Since experiment S-11 showed no oxygen in the outlet gas, we conclude that combustion of oil, as well as carbon, was occurring. This explains why the plateau temperature in the actual retorting should be higher than that calculated for the combustion of a pyrolyzed shale. This higher temperature causes a complete decomposition of the calcite in experiment S-11. Braun's model predicts a value for the oxygen fraction used to burn the oil that is very close to the value of the oxygen breakthrough (η_s) obtained by our model.

For the case of $\beta > 1$ and $N_{d3} < 1$ the establishment of a fully developed profile needs considerable time and, therefore, a longer reactor than has been used in experiments. Braun's model is used to simulate the retorting of a shale with properties similar to the shale used in experiment S-19 by Lawrence Livermore Laboratory. The retorting gas contained 2.5% O_2 by volume. The results of this simulation are presented in Figure 12 and Table 6. Our calculations for the same shale, minus the kerogen, are summarized in Figure 4 and Table 6. A comparison of these two calculations indicates a

TABLE 6. OUR MODEL CALCULATIONS VS. BRAUN MODEL PREDICTIONS

	Combustion of Pyrolysed Shale (Fig. 4)	Braun's Model* for Combustion Retorting (Fig. 12)
ψ_s	0.20	0.26
V (m/h)	0.062	0.065
T_p (K)	791	570
b	1.15	1.14
δ_s	0.00	0.00
γ_s	0.87	0.80

* Braun (1981).

disagreement in the plateau temperature, T_p. In the front part of the thermal wave the gas is heating up the raw solid to a temperature at which the first endothermic reaction takes place. In the case of the raw shale this is the kerogen decomposition, which starts around 570 K. For processed shale the dolomite decomposition, which starts around 790 K, is the first endothermic reaction. Because the heating front is moving faster than the decomposition front, they separate. This separation corresponds to a plateau in the temperature profile at the temperature at which the decomposition starts (570 K for the kerogen, 790 K for the dolomite).

In the case $\beta > 1$, $N_{d3} > 1$ the fully developed profile takes so long to develop that experimental results are not available with which to compare our model. An attempt to use Braun's model to calculate the fully developed profile for this case was not successful because numerical instabilities developed in the calculation.

Effect of CO_2 Effusion

A previous section discussed the case of the inhibition of the O_2 diffusion due to the CO_2 generated from the carbonate decomposition. If a correction factor in the oxygen diffusion coefficient is included in order to take this into account (Sohn and Braun, 1982) the temperature and composition profile presented in Figure 1b and in Table 3 are calculated. If this correction is not included for the same case, the results presented in Figure 1a and Table 3 are obtained. The experimental results for a similar case are presented in Table 5. Both the oxygen breakthrough and the fraction of carbon reacting with CO_2, $(b-1)/b$, calculated without including this correction agree much better with the experimental results. For this reason, the model without the correction was used in all of our calculations.

CONCLUDING REMARKS

A steady state model for the combustion of pyrolyzed shale has been found to provide a better understanding of the process. By considering the fully developed temperature and composition profiles that establish after the combustion wave has moved through a considerable length of the bed, we are able to relate the structure of the temperature profile to the various reactions that are occurring, and in particular to show the separation of different reaction fronts. This has not been possible with unsteady state models because the computational time required to reach the fully developed regime is quite large.

To our knowledge, experiments have not been performed that will allow direct verification of these results. However, a comparison with the temperature and composition profiles obtained for retorting raw shale shows good agreement, or understandable differences.

ACKNOWLEDGMENT

The authors gratefully acknowledge support for this work received from the Shell Companies Foundation. We also want to thank R. L. Braun for providing us with a copy of his computer model developed in the Lawrence Livermore Laboratory.

APPENDIX 1. NUMERICAL CALCULATIONS

Solution of Heat Balance Equations without Chemical Reaction ($r_l = 0$)

The temperature profiles in zones I and III in Figures 1–6 are obtained by solving Eqs. 28–31 for the case of $r_l = 0$. In HH-1 it is shown that for a given temperature wave, steady state temperature profiles cannot exist for both zones I and III. For $\beta > 1$, zone I is steady and zone III is unsteady; for $\beta >$ zone III is steady and zone I is unsteady.

The steady state profiles are described by the following equations:

$$T_g = P + S \exp(-\alpha x), \tag{39}$$

$$T_s = P + S\beta \exp(-\alpha x), \tag{40}$$

with

$$\alpha = (1-\beta)\frac{h_{gs}a_p(1-\epsilon)A}{\dot{m}_g C_g}, \tag{41}$$

$$\beta = \dot{m}_g C_g / V\rho_s C_s (1-\epsilon)A. \tag{42}$$

The parameters P and S are constants obtained by matching the temperature profiles in this zone with the temperature profiles in the adjacent reaction zone.

The unsteady state temperature profiles are obtained by solving numerically Eqs. 28 and 29 with $r_i = 0$. Details about these numerical solutions and their matching to the adjacent reaction zone are given in HH-1.

Steady State Reaction Zone

The reactions occurring in the solids are analyzed by assuming that the particles behave the same as spheres of radius R_p small enough to be isothermal and homogeneous in composition.

The rate of carbon combustion according to Eq. 1 is calculated by the expression

$$r_1 = \frac{\partial \dot{\psi}}{\partial t}\text{comb} = \frac{-9\rho_g N_o}{8\chi_s\rho_s R_p}\left[\frac{\eta}{\dfrac{R_p\psi^{-1/3}-1}{D_e} + \dfrac{3\rho N_g \psi_o^{-2/3}}{8\chi_s\rho_s R_p A_1 \exp(-E_1/RT_s)} + \dfrac{1}{K_g}}\right] \tag{43}$$

This uses kinetics for the reaction as being first-order in oxygen and carbon and pictures the burning of carbon as occurring on the surface of a shrinking core of carbon. The second term in the denominator contains the kinetic parameters, A_1 and E_1, characterizing the rate of reaction. The first and third terms dictate the change of the oxygen concentration from the flow stream to the burning carbon core. The third term represents the gas phase resistance to oxygen diffusion on the outside of the particle. The first term models the diffusion of oxygen through the porous burned solid. The variable $(\psi^{-1/3}-1)$ indicates the increase of the diffusion path as the carbon is consumed and D_e is the effective diffusion coefficient. Mallon and Braun (1976) determined D_e for a Green River shale. They found

$$D_e = 1.48\ 10^{-5}\ \chi_k^2 T_s^{1.7}, \tag{44}$$

where D_e is expressed in m^2/h and χ_k is the weight fraction of

kerogen in the raw shale. For Green River shale this is related to the Fisher assay by the following equation determined by Probstein and Hicks (1982):

$$\chi_\kappa = \frac{\text{Fisher assay } \frac{\text{lt}}{\text{ton}} + 10.8}{8.22} \tag{45}$$

For the cases where the combustion and decomposition zones are combined ($\beta < 1$ and $\beta > 1$ with $N_{d3} < 1$), the carbonate decomposition generates a gas flow inside the particle which could hinder the diffusion of the oxygen. In order to explore this effect for one case (Figure 1b) a method for correcting the effective diffusion coefficient developed by Sohn and Braun (1982) was used. The basic assumption is that the paths for the oxygen diffusion and the outward flow of evolved gas are the same.

The rate of carbon gasification by carbon dioxide, Eq. 2, is represented by the following expression developed by Ergun (1956):

$$r_2 = \left(\frac{\partial \psi}{\partial t}\right)_{\text{gasif.}} = -\frac{\psi A_2 \exp(-E_2/RT_s)}{1 + \frac{\xi}{K_{\text{eq}}\theta}}, \tag{46}$$

where $K_{\text{eq}} = 4.15\ 10^3 \exp(-11{,}400/T_s)$, θ is the weight fraction of CO_2 in the gas, and ξ is the weight fraction of CO.

The scheme proposed by Braun (1981) is used to describe the rates of dolomite and calcite decomposition.

$$\text{Dolomite: } r_3 = \frac{\partial \delta}{\partial t} = -k_3\delta \tag{47}$$

$$\text{Calcite: } r_4 = \frac{\partial \delta}{\partial t} = -k_4\gamma, \tag{48}$$

where δ is the fraction of dolomite remaining, and γ is the fraction of calcite remaining.

Case of $\beta < 1$ and $\beta > 1$, $N_{d3} < 1$

In the cases $\beta < 1$ and $\beta > 1$, $N_{d3} < 1$, all the reactions take place in the same zone (zone II) moving with a velocity V. The steady state mass balance equations for these cases are as follows:

$$\text{Carbon: } \frac{d\psi}{dx} = -\frac{r_1 + r_2}{V} \tag{49}$$

$$\text{Oxygen: } \frac{d\eta}{dx} = -\frac{8\chi_s\rho_s(1-\epsilon)A}{3\dot{m}_g N_o} r_1 \tag{50}$$

$$\text{Dolomite: } \frac{d\delta}{dx} = -\frac{r_3}{V} \tag{51}$$

$$\text{Calcite: } \frac{d\gamma}{dx} = -\frac{r_4}{V} \tag{52}$$

$$\text{Carbon Dioxide: } \frac{d\theta}{dx} = -\frac{44\rho_s(1-\epsilon)A}{\dot{m}_g}\left[\frac{r_3\chi_d}{84} + \frac{r_4\chi_c}{100} - \frac{(r_1 - r_2)\chi_s}{12}\right] \tag{53}$$

$$\text{Carbon Monoxide: } \frac{d\xi}{dx} = -\frac{28\chi_s\rho_s(1-\epsilon)A}{6\dot{m}_g} r_2 \tag{54}$$

The temperature and concentration profiles are calculated by using shooting methods (Scheid, 1968) to solve Eqs. 30, 31, and 49–54, with the following boundary conditions:

For $\beta < 1$

$x = \infty$ $\quad T_s = T_g = T_f$

$x = 0$ $\quad \psi = 1$

$\delta = 1$

$\gamma = 1$

$x = \hat{x}$ $\quad T_s = T_g$: from matching with zone I

$\eta = 1$

$\psi = 0$: no breakthrough

$\theta = 0$

$\xi = 0$

$r_3 = 0$: no more decomposition

$r_4 = 0$:

For $\beta > 1$, $N_{d3} < 1$

$x = 0$ $\quad T_s = T_g = T_{di}$: from matching with zone II

$r_3 = 0$

$\psi = 1$

$\delta = 1$

$\gamma = 1$

$\eta = 0$: no O_2 breakthrough

$x = \hat{x}$ $\quad \eta = 1$

$\theta = 0$

$\xi = 0$

$x = -\infty$ $\quad T_s = T_g = T_i$

The nonlinearity of the equations and the sensitivity of the numerical computations to round off errors required the use of double precision numerics and the method of Gear (1971) for the numerical integration. More details regarding these methods are given in Appendices 2 and 3.

Case of $\beta > 1$, $N_{d3} > 1$

In this case the combustion front (zone IIa) is completely separated from the decomposition front (zone IIc). These two fronts move apart at a velocity $V_{cd} - V$ given by Eqs. 21 and 16. Consequently these two reaction zones have to be treated separately.

In order to calculate the properties of the decomposition zone (IIc), a coordinate system moving at a velocity V_{cd} is used. The heat balance equations are the same as Eqs. 30 and 31 with V_{cd} substituted for V. The reactions that occur in this zone are the gasification of the carbon with CO_2 produced by carbonate decomposition,

$$\frac{d\psi}{dx} = -\frac{r_2}{V_{cd}}, \tag{55}$$

and the decompositions of dolomite and calcite, given by Eqs. 51 and 52 with V_{cd} substituted for V. The carbon monoxide balance is given by Eq. 54 and the carbon dioxide balance, by

$$\frac{d\theta}{dx} = -\frac{44\rho_s(1-\epsilon)A}{\dot{m}_g}\left[\frac{r_3\chi_d}{84} + \frac{r_4\chi_c}{100} - \frac{r_2\chi_s}{12}\right] \tag{56}$$

The boundary conditions used to calculate this zone are as follows:
At the beginning of the zone

$$x = x_i \quad T_s = T_g = T_{di}$$
$$\psi = 1$$
$$\delta = 1$$
$$\gamma = 1$$

At the end of the zone

$x = x_s$ $T_s = T_g = T_m$ from matching with zone IIa, Eq. 27
$\theta = 0$
$\xi = \xi_{eq}$: CO coming from zone IIa
$\delta = 0$
$\gamma = 0$

Note that the oxygen concentration in this zone is zero.

For the case $\beta > 1$, $N_{d3} > 1$, the combustion zone (IIa) moves at velocity V, given by Eq. 16. The carbon that remains after the gasification reaction that takes place in the decomposition zone will be burned to produce CO_2, which in turn can react with the carbon to produce CO. Since the temperature at the end of the combustion zone is high enough and the retention time is very long, the reaction between C and CO_2 comes to equilibrium, so the portion of carbon that reacts with CO_2 is obtained from equilibrium considerations. To simplify the calculations the carbon combustion (Reaction 1) and the carbon gasification by CO_2 (Reaction 2) are combined as follows:

$$cC + O_2 \rightarrow 2(c-1)CO + (2-c)CO_2 \tag{57}$$

The rate limiting step of this reaction is the diffusion of oxygen through the burned shale. Therefore the rate expression for Eq. 57, r_5, is given by Eq. 43 with cN_o substituted for N_o. Because at the end of the combustion zone the temperature T_m is high and the gas-solid contact time is enough to achieve equilibrium between C—CO—CO_2, the final value of c can be calculated from equilibrium considerations (Yoon et al., 1978):

$$\frac{(c-1)^2}{2-c} = 1.222\ 10^9 \exp\left(-\frac{20{,}282}{T_m}\right) \tag{58}$$

In order to simplify the calculations this final value of c is taken to be the average value. This is not perfectly correct because the value of c near $x = x_f$ would be less than the value adopted (low temperature, low CO_2 concentration). Because of the low endothermic effect of the gasification reaction compared to the exothermic combustion, the adoption of an average value for c will not affect the temperature profile significantly.

$$|\Delta H_5| = \frac{1}{c}|\Delta H_1| - \frac{c-1}{c}|\Delta H_2| \tag{59}$$

In the mass balance equations new ψ anda $\chi(\psi'$ and $\chi')$ are defined because the solid remaining after the decomposition zone contains a weight fraction, χ_s', of carbon. The fraction of χ_s' remaining is defined as ψ' and the fraction of χ_s' remaining unburned at the end of the combustion as ψ_s'. The mass balances become

$$\text{Carbon: } \frac{d\psi'}{dx} = -\frac{r_5}{V}, \tag{60}$$

$$\text{Oxygen: } \frac{d\eta}{dx} = -\frac{8\chi_s'\rho_s(1-\epsilon)Ar_5}{3c\dot{m}_g N_o}. \tag{61}$$

The heat and mass balance equations are solved simultaneously to obtain the temperature and concentration profiles in zone IIa. The boundary conditions to be satisfied are as follows:

$$x = 0 \quad T_s = T_g = T_m$$
$$\psi' = 1$$
$$\eta = 0$$
$$x = x_f \quad \eta = 1$$
$$x = -\infty \quad T_s = T_g = T_i$$

A difficulty is that the solutions for zones IIa and IIc are not decoupled since the carbon burned in zone IIa is the carbon remaining after the gasification reaction in zone IIc. Therefore solutions for zones IIa and IIc were obtained simultaneously using an iterative procedure described in Appendix 4.

APPENDIX 2

Solution of the Steady State Temperature and Composition Profile for $\beta < 1$

The solution of Eqs. 30, 31, and 49–54 requires guessing four parameters: η_s (oxygen breakthrough), b (moles of C reacting per mole of O_2), calcite remaining, γ_s, and the dolmite remaining, δ_s. The boundary conditions for $x = \infty$ are as follows:

$$T_s = T_g = T_f$$
$$\psi = 1$$
$$\delta = 1$$
$$\gamma = 1$$
$$\eta = \eta_s\text{: to guess}$$

$$\theta = \theta_s = \frac{44\rho_s(1-\epsilon)}{\frac{\dot{m}_g}{A}}\left[\frac{\chi_s(1-\psi_s)(2-b)}{12b} + \frac{\chi_d(1-\delta_s)}{84} + \frac{\chi_c(1-\gamma_s)}{100}\right] \tag{1'}$$

$$\xi = \xi_s = \frac{28\chi_s(1-\psi_s)(b-1)V\rho_s(1-\epsilon)}{6\frac{\dot{m}_g}{A}b} \tag{2'}$$

In the case of $N_d2 > 1$, $\delta_s = 0$, $\gamma_s = 0$. In the case of $N_{d2} > 1$, the overall heat balances, Eqs. 22 and 23, give an estimate of δ_s and γ_s. This makes the convergence of the solution easier.

The integration of the system is stopped at $d\delta/dx = 0$ and $d\gamma/dx = 0$, and η_s is adjusted to satisfy $\psi = 0$ $\eta = 1$, and b to satisfy $T_s = T_g$ at $x = \hat{x}$.

APPENDIX 3

Solution of the Steady State Temperature and Composition Profile for $\beta > 1$, $N_{d3} < 1$

Equations 30, 31, and 49–54 are solved by guessing four parameters: η_s, b, δ_s, γ_s, asa in the case $\beta < 1$. By an overall mass balance, Eqs. 25 and 26, the values of δ_s and γ_s are estimated.

The boundary conditions at $x = 0$ are as follows:

$$T_s = T_g = T_{di}\text{: (enough to have } d\delta/dx = 0)$$
$$\psi = 1$$
$$\delta = 1$$
$$\gamma = 1$$
$$\eta = 0$$

$$\theta = \theta_s\text{: from Eq. 1'}$$

$$\xi = \xi_s\text{: from Eq. 2'}$$

$$r_3 = 0$$

At the beginning of the integration ($x = 0$) we impose the condition of $r_1 = 0$ till $x < \hat{x}$ *guess*. The reason for this is that the combustion starts later than the decomposition because all the oxygen is depleted before the gas reached $x = 0$. The integration is stopped at $x = \hat{x}$ where $\xi = 0$. Parameter b is adjuted to obtain $\xi = 0$ at the end of the integration. Then $\hat{x}$ is adjusted to obtain $\eta = 1$ and ψ_s is adjusted to obtain $\psi = \psi_s$ at the end of the integration.

APPENDIX 4

Solution of the Steady State Temperature and Composition Profile for $\beta > 1$, $N_{d3} > 1$

For this case solutions are obtained from two zones, IIa and IIc. For the combustion zone IIa Eqs. 30, 31, 58, 60, and 61 are solved. The integration is started with the conditions,

$$T_s = T_g = T_m = T_i + \frac{\Delta H_5 \chi_s'(1 - \psi_s')}{C_s(1 - \beta)}$$

$$\psi' = 1$$

$$\eta = 0$$

We guess c and ψ_s' and stop the integration at $T_s = T_g$. Then we adjust ψ_s' in order to obtain at the end of the integration $T_s = T_g = T_i$ and $\psi' = \psi_s'$. For the decomposition zone IIc, Eqs. 30, 31, 51, and 52 with V_{cd} for V, and Eqs. 55 and 56 are solved. The integration is started at $x = x_i$ with the following conditions:

$$T_s = T_g = T_{di}\text{ (such as } d\delta/dx \simeq 0)$$

$$\psi = 1$$

$$\delta = 1$$

$$\gamma = 1$$

$$\theta = \theta_s\text{: from Eq. 1'}$$

$$\xi = \xi_s\text{: from Eq. 2'}$$

The integration is stopped at $T_s = T_g$. The value of b is adjusted so as to match the value of ξ obtained at the end of the combustion zone, IIa. The new guess of b changes the profiles of zone IIa. Therefore the new iteration is started by integrating the equation for zone IIa. Note that the ψ used in the decomposition zone is not the same as the ψ' used in the combustion zone (at $x = x_i$, $\psi = 1$, and $x = 0$, $\psi' = 1$).

NOTATION

A_i = preexponential factor in the rate equation for reaction i
A = area of bed section
a_p = ratio of the particle area to its volume
b = moles of carbon consumed per mole of oxygen during combustion retorting
c = stoichiometric factor for the reaction: $cCO + O_2 \rightarrow 2(c-1)CO + (2-c)CO_2$
C_g = heat capacity of the gas
C_s = heat capacity of the solid
D_e = effective diffusion coefficient of oxygen through the burned shale
$\overline{D}_e$ = average value of D_e
E_i = activation energy for reaction i
h_{gs} = overall gas-solid heat transfer coefficient
i = 1 for reaction $C + O_2 \rightarrow CO_2$
2 for reaction $C + CO_2 \rightarrow 2CO$
3 for dolomite decomposition
4 for calcite decomposition
5 for reaction $cCO + O_2 \rightarrow 2(c-1)CO + (2-c)CO_2$
K_g = mass transfer coefficient through the gas film surrounding the particle
k_i = rate constant for reaction i
$\dot{m}_g$ = mass flux of the gas
N_o = weight fraction of oxygen in the gas in the entry section
R = universal gas constant
R_p = particle radius
r_i = rate of reaction i
T_{cf} = temperature at which calcite stops decomposing
T_{ci} = temperature at which calcite starts decomposing
T_{df} = temperature at which dolomite stops decomposing
T_{di} = temperature at which dolomite starts decomposing
T_f = initial temperature of the bed

$$T_{ad} = T_f + \frac{|\Delta H_c|\chi_s - |\Delta H_3|\chi_d}{C_s(1-\beta)} \text{ for } \beta < 1$$

$$= T_i + \frac{|\Delta H_c|\chi_s(1-\psi_s) - |\Delta H_3|\chi_d}{C_s(\beta - 1)} \text{ for } \beta > 1$$

$$T_{adc} = T_f + \frac{|\Delta H_c|\chi_s - |\Delta H_3|\chi_d - |\Delta H_4|\chi_c}{C_s(1-\beta)} \text{ for } \beta < 1$$

$$= T_i + \frac{|\Delta H_c|\chi_s(1-\psi_s) - |\Delta H_3|\chi_d - |\Delta H_4|\chi_c}{C_s(\beta - 1)} \text{ for } \beta > 1$$

T_g = gas temperature
T_i = gas temperature at the entry section
T_m = maximum temperature
T_p = plateau temperature
T_s = solid temperature
t = time
V = combustion front velocity
V_c = calcite decomposition front velocity
V_{cd} = carbonate decomposition front velocity
V_d = dolomite decomposition front velocity
V_{us} = unsteady state heating zone velocity
x = length in the bed
$\hat{x}$ = length of the reaction zone
$\hat{x}$ = position where the combustion starts in the case $\beta > 1$, $N_{d3} < 1$
x_f = end of the combustion zone for the case $\beta > 1$, $N_{d3} > 1$
x_i = beginning of the decomposition zone for the case $\beta > 1$, $N_{d3} > 1$
x_s = end of the decomposition zone for the case $\beta > 1$, $N_{d3} > 1$
z = distance from the entry of the bed

Greek Letters

$\alpha = (1-\beta)\dfrac{h_{gs}a_p(1-\epsilon)A}{\dot{m}_g C_g}$

β = ratio of heat capacity rates $\dfrac{\dot{m}_g C_g}{V\rho_s C_s(1-\epsilon)A}$

β_m = modified beta $\dfrac{8\chi_s C_g}{3N_o C_s}$

γ = fraction of calcite remaining
γ_s = fraction of calcite remaining at the end of the operation
δ = fraction of dolomite remaining

δ_s = fraction of dolomite remaining at the end of the operation
$\Delta H_c = |\Delta H_1 + (b-1)\Delta H_2|/b$
$\Delta H_5 = |\Delta H_1 + (c-1)\Delta H_2|/c$
ΔH_i = heat of reaction i
ϵ = void fraction
η = fraction of oxygen remaining
η_s = fraction of oxygen remaining at the end of the bed (oxygen breakthrough)
θ = weight fraction of CO_2 in the gas
θ_s = weight fraction of CO_2 in the gas at the exit
ξ = weight fraction of CO in the gas
ξ_s = weight fraction of CO in the gas at the exit
ρ_g = density of the gas
ρ_s = density of the solid
χ_c = weight fraction of calcite in the processed shale
χ_d = weight fraction of dolomite in the processed shale
χ_s = weight fraction of carbon in the processed shale
χ_s' = weight fraction of carbon in the shale before the combustion zone IIa, in the case $\beta > 1$, $N_{d3} > 1$
χ_k = weight fraction of kerogen in the raw shale
ψ = fraction of carbon remaining
ψ' = fraction of χ_s remaining for the combustion zone IIa, in the case of $\beta > 1$, $N_{d3} > 1$
ψ_s = carbon breakthrough
ψ_s' = fraction of χ_s remaining unburned at the end of the combustion zone IIa in the case $\beta > 1$, $N_{d3} > 1$

Dimensionless Parameters

$$N_{d1} = \frac{T_{ad}}{T_{df}}$$

$$N_{d2} = \frac{T_{adc}}{T_{cf}}$$

$$N_{d2m} = \frac{T_f}{1{,}000} + \frac{|\Delta H_1|\chi_s - |\Delta H_3|\chi_d - |\Delta H_4|\chi_c}{1{,}000 C_s(1-\beta_m)}$$

$$N_h = \frac{h_{gs} a_p R_p^2}{\overline{D}_e C_g \rho_g}$$

$$N_{d3} = \frac{T_{adc}}{T_{di}}$$

$$N_{d4} = \frac{T_{ad}}{T_{di}}$$

$$N_{d3m} = \frac{T_i}{800} + \frac{|\Delta H_1|\chi_s - |\Delta H_3|\chi_d - |\Delta H_4|\chi_c}{800 C_s(\beta_m - 1)}$$

$$N'_{d3m} = \frac{T_i}{800} + \frac{|\Delta H_1 + \Delta H_2|\chi_s - |\Delta H_3|\chi_d - |\Delta H_4|\chi_c}{800 C_s(2\beta_m - 1)}$$

$$N_{Tf} = \frac{T_f R}{E_1}$$

$$N_{Ti} = \frac{T_i R}{E_1}$$

LITERATURE CITED

Baer, A. D., and C. A. Dahl, "A Simple Semisteady-State Model of the Combustion Retort," *In Situ*, 4(1), 79 (1980).

Braun, R. L., "Mathematical Modeling of Modified In Situ and Aboveground Oil Shale Retorting," URCL-53119, Lawrence Livermore Laboratory, Livermore, CA (1981).

Campbell, J. H., "Kinetics of Decomposition of Colorado Oil Shale. 2: Carbonate Minerals," URCL-52089 (Pt 2), Lawrence Livermore Laboratory, Livermore, CA (1978).

———, "Modified In Situ Retorting: Results from LLNL Pilot Retorting Experiments," UCRL-53168, Lawrence Livermore Laboratory, Livermore, CA (1981).

Campbell, J. H., and A. K. Burnham, "Reaction Kinetics for Modeling Oil Shale Retorting," UCRL-81622, Lawrence Livermore Laboratory, Livermore, CA (1979).

Carnahan, B., H. A. Luther, and J. O. Wilkes, *Applied Numerical Methods*, 407, John Wiley & Sons, New York (1976).

DeAcetis, J., and C. Thodos, "Mass and Heat Transfer in Flow of Gases through Spherical Packings," *Ind. Eng. Chem.*, **52**, 1,003 (1960).

Ergun, S., "Kinetic of the Reaction of Carbon Dioxide with Carbon," *J. Phys. Chem.*, **60**, 480 (1956).

Gear, C. W., *Numerical Initial Value Problems in Ordinary Differential Equations*, Prentice-Hall, Englewood Cliffs, NJ (1971).

Gregg, D. W., and T. F. Edgar, "Underground Coal Gasification," *AIChE J.*, **24**(5), 753 (1978).

Hiskakis, M., and T. J. Hanratty [HH-1], "Combustion of Carbon Residue from Oil Shale Retorting," *AIChE J.*, **29**(3), 451 (1983).

Mallon, R. C., and R. L. Braun, "Reactivity of Oil Shale Carbonaceous Residue with Oxygen and Carbon Dioxide," *Colorado School of Mines Qtly.*, **71**(4), 309 (1976).

Perry and Chilton, *Chemical Engineers Handbook*, 5th Ed., McGraw-Hill, New York (1969).

Probstein, R. F., and R. E. Hicks, *Synthetic Fuels*, 322, McGraw-Hill, New York (1982).

Scheid, F., *Numerical Analysis*, McGraw-Hill, New York (1968).

Sohn, H. Y., and K. S. Kim, "Intrinsic Kinetics of the Reaction between Oxygen and Carbonaceous Residue in Retorted Oil Shale," *Ind. Eng. Chem. Proc. Des. Dev.*, **19**(4), 550 (1980).

Sohn, H. Y., and R. L. Braun, "The Effect of Internally Generated Bulk Flow on the Rates of Gas-Solid Reactions. 1: Development of an Approximate Solution," UCRL-87976, Lawrence Livermore Laboratory, Livermore, CA (1982).

Yoon, H., J. Wei, M. Denn, "A Model For Moving Bed Coal Gasification Reactors," *AIChE J.* **24**(5), 885 (1978).

Manuscript received Jan. 5, 1984; revision received Oct. 9 and accepted Oct. 15, 1984.